3502 *Chem. Mater.* **2010,** *22,* 3502–3510
DOI:10.1021/cm100627g

CHEMISTRY OF MATERIALS
Article

Toward a Low-Temperature Sol−Gel Synthesis of TiO_2(B) Using Mixtures of Surfactants and Ionic Liquids

Helena Kaper,[†,‡] Sébastien Sallard,[§] Igor Djerdj,[⊥,#] Markus Antonietti,[∥] and Bernd M. Smarsly*[,§]

[†]*Institute of Bioengineering and Nanotechnology, 31 Biopolis Way, The Nanos, Singapore 138669,* [‡]*ICSM, UMR 5257, Institut de Chimie Séparative de Marcoule, Site Marcoule, BP 17171, F-30207 Bagnols Sur Ceze, France,* [§]*Institute of Physical Chemistry, University of Giessen, Heinrich-Buff-Ring 58, D-35392 Giessen, Germany,* [⊥]*Ruđer Bošković Institute, Bijenička 54, 10000, Zagreb, Croatia,* [∥]*Max-Planck Institute of Colloids and Interfaces, Am Mühlenberg 1, D-14424 Potsdam, Germany, and* [#]*Department of Materials, ETH Zürich, Wolfgang-Pauli-Strasse 10, 8093 Zürich, Switzerland*

Received March 1, 2010

An approach toward the synthesis of nanocrystalline TiO_2(B) in surfactant/ionic liquid systems at low temperature (100 °C) by means of sol−gel chemistry is presented. As reaction medium, a solution of imidazolium- and ammonium-based surfactants in ionic liquids was applied. Interestingly, TiO_2(B), in coexistence with anatase, was observed only in cases where the ionic liquid is based on imidazolium moieties. The final product contained up to 60 wt % TiO_2(B), depending on the initial amount of surfactant. X-ray powder diffraction measurements and transmission electron microscopy revealed small particle sizes (ca. 2 nm for TiO_2(B), around 6 nm for anatase) as well as a high crystallinity of the material. The materials possessed surface areas up to 300 m^2/g. Electrochemical studies further confirmed the presence of the two titania polymorphs anatase and TiO_2(B) in similar proportions. Small-angle X-ray scattering experiments gave insight into the phase behavior of the surfactant in the ionic liquid under reaction conditions. The formation of TiO_2(B) is discussed based on systematic variation of diverse parameters.

1. Introduction

Nanosized titanium dioxide (TiO_2) is one of the most studied metal oxides in materials science because of its wide range of application, e.g., as photocatalyst, electrode material or semiconductor . Among the nine known polymorphs of titania, anatase and rutile stand out with a broad variety of synthesis strategies, whereas only a few examples on the preparation of the more exotic modification TiO_2(B) are known. The general synthesis way, as reported in the early 1980s by Marchand et al., is based on ion exchange and calcination of layered titanates such as $K_2Ti_4O_9$.[1,2] Thereby, TiO_2(B) nanotubes are obtained. Bruce et al.[3] developed a hydrothermal method using commercial anatase to synthesize TiO_2(B) nanowires and nanotubes. The synthesis of TiO_2(B) in form of nanoparticles has only recently been described by Kobayashi et al. via a hydrothermal method.[4] Next to that, TiO_2(B) is found as undesired side product in the synthesis of titania nanotubes[5−7] and titania thin films.[8,9] Because of the open structure of TiO_2(B),[10] this polymorph of TiO_2 has complementary interesting properties, especially as lithium ion electrode[11−13] and photocatalytic active material.[14,15] Nanosized TiO_2 is an attractive alternative to graphite as negative electrode (anode) in the Li-ion rechargeable battery.[16] Similar to graphite, titania is abundant, inexpensive and environmentally friendly. Moreover, the low redox potential (1.5 V versus Li^+/Li) of titania offers a safer Li-ion battery by avoiding electroplating of lithium on the electrode. As a major drawback, the Li-insertion capacity is usually much smaller for titania than for graphite. To improve the capacity to store lithium in titania, the ability to tailor the titania

*Corresponding author. E-mail: bernd.smarsly@phys.chemie.uni-giessen.de.

(1) Marchand, R.; Brohan, L.; Tournoux, M. *Mater. Res. Bull.* **1980**, *15*, 1129–1133.
(2) Brohan, L.; Verbaere, A.; Tournoux, M.; Demazeau, G. *Mater. Res. Bull.* **1982**, *17*, 355–361.
(3) Armstrong, A. R.; Armstrong, G.; Canales, J.; Bruce, P. G. *Angew. Chem., Int. Ed.* **2004**, *43*, 2286–2288.
(4) Kobayashi, M.; Petrykin, V. V.; Kakihana, M. *Chem. Mater.* **2007**, *19*, 5373–5376.
(5) Kasuga, T.; Hiramatsu, M.; Hoson, A.; Sekino, T.; Niihara, K. *Langmuir* **1998**, *14*, 3160–3163.
(6) Kavan, L.; Kalbac, M.; Zukalova, M.; Exnar, I.; Lorenzen, V.; Nesper, R.; Graetzel, M. *Chem. Mater.* **2004**, *16*, 477–485.
(7) Nishizawa, H.; Aoki, Y. *Solid State Chem.* **1985**, *56*, 158–165.
(8) Wang, K. X.; Morris, M. A.; Holmes, J. D. *Chem. Mater.* **2005**, *17*, 1269–1271.
(9) Kavan, L.; Rathousky, J.; Grätzel, M.; Shklover, V.; Zukal, A. *J. Phys. Chem. B* **2000**, *104*, 12012–12020.
(10) Tournoux, M.; Marchand, R.; Brohan, L. *Prog. Solid State Chem.* **1986**, *17*, 33–52.
(11) Zukalová, M.; Kalbac, M.; Kavan, L.; Exnar, I.; Graetzel, M. *Chem. Mater.* **2005**, *17*, 1248–1255.
(12) Armstrong, G.; Armstrong, A. R.; Canales, J.; Bruce, P. G. *Electrochem. Solid-State Lett.* **2006**, *9*, A139–A143.
(13) Armstrong, A. R.; Armstrong, G.; Canales, J.; Garcia, R.; Bruce, P. G. *Adv. Mater.* **2005**, *17*, 862–685.
(14) Zukalová, M.; Kalbac, M.; Kavan, L.; Exnar, I.; Haeger, A.; Graetzel, M. *Prog. Solid State Chem.* **2005**, *33*, 253–261.
(15) Kuo, H. L.; Kuo, C. Y.; Liu, C. H.; Chao, J. H.; Lin, C. H. *Catal. Lett.* **2007**, *113*, 7–12.
(16) Bruce, P. G.; Scrosati, B.; Tarascon, J. M. *Angew. Chem., Int. Ed.* **2008**, *47*, 2930–2946.

 Published on Web 05/13/2010

Scheme 1. Molecular Structure of ionic Liquids and Surfactants Employed in This Work: 1-Butyl-3-methyl-imidazolium Tetrafluoroborate (C_4mimBF_4), 1-Butyl-3-methyl-imidazolium Tetrafluoroborate (C_4mimBF_4), 1-Hexadecyl-3-methylimidazolium Chloride (C_{16}mimCl), Ethylammonium Nitrate (EAN) and Hexadecyltrimethylammonium Chloride (CTAC)

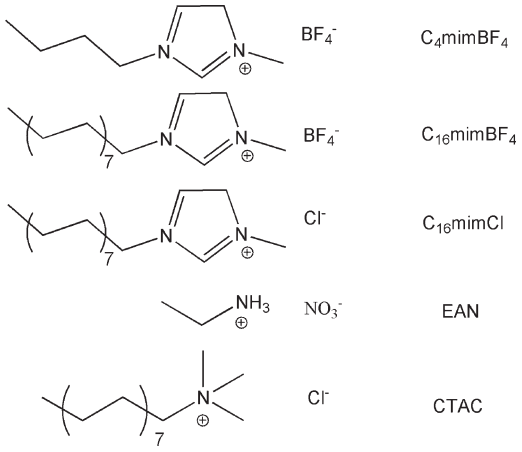

material with respect to size, shape, and morphology comes into play, as these factors show a major influence on the charge capacity. Anatase and rutile are limited to a doping of $x = 0.5$ (Li_xTiO_2, 165 mA h g^{-1})[13] and $x = 0.6$ (Li_xTiO_2, 200 mA h g^{-1})[17] respectively, whereas TiO_2(B) nanowires allow a higher charge capacity of $x = 0.91$ (305 mA h g^{-1}).[13]

Herein, we report a low-temperature sol−gel−based synthesis of mixtures of TiO_2(B) and anatase in ionic liquids (ILs). Ionic liquids are organic salts with a low melting temperature (generally below 373 K) that offer unique solvent properties because they consist solely of ions. In sol−gel chemistry, they have been used as solvent or solvent template for the synthesis of metal oxides such as ZnO, V_2O_5, and TiO_2. In the case of TiO_2, next to various synthesis ways toward anatase,[18−20] the direct synthesis of rutile at low temperature was reported recently.[17,21] So far, titania was synthesized in the pure ionic liquid as solvent or solvent template. It was found[17] that the formation of crystalline TiO_2 in ILs is governed by the peculiar charge distribution and interaction between the IL and the titania surface. In the here-presented approach, surfactants such as hexadecyltrimethylammonium chloride (CTAC) or the long-chain ionic liquid 1-hexadecyl-3-methylimidazolium chloride (C_{16}mimCl) are added to the reaction mixture. In sol−gel chemistry, surfactants are used because of their ability to form micelles and higher ordered structures in water, but also to stabilize materials interfaces.[22] Similar to the phase behavior of surfactants in water, surfactants form micelles as well as higher-ordered structures in ionic liquids. The formation of micelles in one of the oldest known ionic liquids, ethylammonium nitrate (EAN), has already been reported in the beginning of the 1980s.[23,24] Recently, the formation of aggregates of nonionic and ionic surfactants in ionic liquids has been investigated.[25,26] Here, we want to explore the use of such an ionic liquid−surfactant system as a reaction medium, thus offering innovative pathways in the synthesis of nanostructures. For that, two types of solvent property donating moieties were examined, namely the imidazolium group as in C_4mimBF_4 and C_{16}mimCl, and the ammonium group as in CTAC and EAN. On the solvent side, 1-butyl-3-methyl-imidazolium tetrafluoroborate (C_4mimBF_4) and ethylammonium nitrate (EAN) (see scheme 1) were used. As IL-based surfactants, CTAC, C_{16}mimCl and C_{16}mimBF_4 were employed. The resulting materials were characterized by means of X-ray powder diffraction (XRD), transmission electron microscopy (TEM), nitrogen sorption as well as cyclic voltammetry and galvanostatic measurements. Small-angle X-ray scattering (SAXS) experiments reveal structural details about the surfactant-ionic liquid mixture.

2. Results and Discussion

2.1. Impact of Synthesis Parameters on the Anatase/TiO_2(B) Ratio. In order to study the influence of the surfactant on the final product, the synthesis was carried out with varying amounts of surfactant in different ionic liquids (ILs). In Table 1, the different compositions with their corresponding products (anatase, TiO_2(B)) are summarized.

First, the system C_{16}mimCl in C_4mimBF_4 is discussed. Pure anatase is formed in sole C_4mimBF_4 without additives. However, mixing with the long tail derivative leads to the formation of TiO_2(B) next to anatase. The content of TiO_2(B) in the final product, as determined by Rietveld analysis from XRD data, apparently depends systematically on the initial ratio of surfactant to IL. Surprisingly, it appears that the maximum fraction of TiO_2(B) is actually achieved at a quite low ratio of C_{16}mimCl/C_4mimBF_4, e.g., at only 10 wt % (sample 2). In general, the ratio of anatase to TiO_2(B) varies between 40 and 60 wt % (samples 2−6). Above a certain concentration, pure anatase is formed again (samples 7 and 8), thus pointing to a key role of solvent structure in the morphosynthetic process.

The situation is different for the mixture of CTAC in C_4mimBF_4 (samples 9−15, Table 1). In this case, TiO_2(B) is formed in only a very limited concentration range (samples 12 and 13), and the amount of TiO_2(B) is lower (around 30 wt % as compared to nearly 60 wt % for C_{16}mimCl/C_4mimBF_4, sample 2). Finally, all systems where the solvent is based on the ammonium group and independent of the

(17) Kaper, H.; Endres, F.; Djerdj, I.; Antonietti, M.; Smarsly, B. M.; Maier, J.; Hu, Y. S. *Small* **2007**, *3*, 1753–1763.
(18) Nakashima, T.; Kimizuka, N. *J. Am. Chem. Soc.* **2003**, *125*, 6386–6387.
(19) Yoo, K. S.; Choi, H.; Dionysiou, D. D. *Catal. Commun.* **2005**, *6*, 259–262.
(20) Zhou, Y.; Antonietti, M. *J. Am. Chem. Soc.* **2003**, *125*, 14960–14961.
(21) Al Zoubi, M.; Farag, H. K.; Endres, F. *Aust. J. Chem.* **2008**, *61*, 704–711.
(22) Kresge, C. T.; Leonowicz, M. E.; Roth, W. J.; Vartuli, J. C.; Beck, J. S. *Nature* **1992**, *359*, 710–712.
(23) Evans, D. F.; Yamauchi, A.; Roman, R.; Casassa, E. Z. *J. Colloid Interface Sci.* **1982**, *88*, 89–96.
(24) Evans, D. F.; Yamauchi, A.; Wei, G. J.; Bloomfield, V. A. *J. Phys. Chem.* **1983**, *87*, 3537–3541.
(25) Thomaier, S.; Kunz, W. *J. Mol. Liq.* **2007**, *130*, 104–107.
(26) Araos, M. U.; Warr, G. G. *J. Phys. Chem. B* **2005**, *109*, 14275–14277.

Table 1. Synthesis of Anatase and Anatase/TiO_2(B) in the Solvent Systems C_{16}mimCl/C_4mimBF_4, CTAC/C_4mimBF_4, C_{16}mimBF_4/C_4mimBF_4, C_{16}mimCl/EAN, and CTAC/EAN

sample	wt % surfactant	product composition	anatase (wt %)[a]	TiO_2(B) (wt %)[a]	D_{anatse} (nm)[b]	$D_{TiO2(B)}$ (nm)[b]	R_{wp} (%)
			C_{16}mimCl + C_4mimBF_4				
1	0	anatase	100	0			
2	10	anatase + TiO_2(B)	43	57	6	1.4	8.9
3	20	anatase + TiO_2(B)	47	53	6.6	1.4	8.6
4	30	anatase + TiO_2(B)	60	40	9	1.3	10.2
5	40	anatase + TiO_2(B)	53	47	8.1	1.8	11.1
6	50	anatase + TiO_2(B)	52	48	8.7	2	10.4
7	60	anatase	100	0	6.7		10.5
8	70	anatase	100	0	7.5		10.3
			CTAC + C_4mimBF_4				
9	10	anatase	100	0	10.6		11.2
10	20	anatase	100	0	5.2		8.8
11	30	anatase + TiO_2(B)	70	30	9.3	1.9	9.7
12	40	anatase + TiO_2(B)	65.0	35.0	7.5	2.3	9.7
13	50	anatase	100	0	6.9		10.9
14	60	anatase	100	0	8.5		10.8
15	70	anatase	100	0	8.7		10.5
			C_{16}mimBF_4 + C_4mimBF_4				
16	10	anatase	100	0	6.8		10.1
17	20	anatase + TiO_2(B)	47	53	10	2.2	13.9
18	30	anatase + TiO_2(B)	48	52	9.1	1.4	9.4
19	40	anatase + TiO_2(B)	51	49	7.8	1	8.13
20	50	anatase + TiO_2(B)	64	36	7.2	1.7	8.8
			C_{16}mimCl + EAN				
21	0	anatase	100	0	3.6		11.1
22	10	anatase	100	0	3.6		8.7
23	20	anatase	100	0	3.9		9.3
24	30	anatase	100	0	3.3		7.9
25	40	anatase	100	0	3.6		10.4
26	50	anatase	100	0			
			CTAC + EAN				
27	10	anatase	100	0	3.7		8.3
28	20	anatase	100	0	2.8		7.6/
29	30	anatase	100	0	3.4		9.1
30	40	anatase	100	0	3.7		9.7
31	50	anatase	100	0	3.6		8.8

[a] The amount of anatase and TiO_2(B) was determined by Rietveld analysis. [b] The average apparent crystallite size was determined by Rietveld analysis.

surfactant structure (C_{16}mimCl/EAN, samples 21−26, Table 1, and CTAC/EAN, samples 27−31, Table 1) produce only pure anatase for any ratio of surfactant/IL. Therefore, the imidazolium group in the solvent phase plays a crucial role, as also seen by the fact that the highest amount of TiO_2(B) in the C_{16}mimCl/C_4mimBF_4 system is achieved at a surprisingly low concentration of surfactant (10 wt %, sample 2).

So far, our study has been focused on the more commonly used surfactants and ionic liquids CTAC and C_4mimBF_4, that is, two different counterions, Cl^- and BF_4^-, are present at the same time. To analyze a potential role of the chlorine in the development of the TiO_2(B) phase, we also studied the system of C_{16}mimBF_4 dispersed in C_4mimBF_4 (samples 16−20, Table 1). This system is simplified to the presence of only one counterion, namely BF_4^-. Also in this case, TiO_2(B) is obtained as a second phase next to anatase. The results are similar to the system C_{16}mimCl in C_4mimBF_4 (samples 2−8, Table 1) with respect to crystallite size and phase composition. One major difference is the evolution of the TiO_2(B) phase only above a surfactant concentration of 10 wt %. At high concentration of C_{16}mimBF_4 in C_4mimBF_4, e.g., above 50%, the solution becomes very viscous, so that the synthesis could not be carried out in the same manner. Therefore, only surfactant concentrations of up to 50 wt % are reported.

2.2. Structural Characterization. The final products were analyzed by XRD and electron microscopy. The X-ray diffraction (XRD) pattern of sample 3 with a anatase (TiO_2(B)) content of 47.5 wt % (52.5 wt %, respectively) together with the assigned Miller indices is shown in Figure 1. To determine the ratio of anatase to TiO_2(B) in the final product as well as the size of the anatase and TiO_2(B) particles, Rietveld analysis of the XRD patterns was carried out using the Rietveld program FULLPROF. Phase composition of the investigated compounds was determined from the refined values of scale factors using Hill and Howard approach.[27] A standard Rietveld fitting assuming isotropic broadening of the peaks due to the small crystallites results in a rather poor agreement between the calculated and experimental profiles. Therefore, an anisotropic line broadening was introduced and was described by a spherical

(27) Hill, R. J.; Howard, C. J. *J. Appl. Crystallogr.* **1987**, *20*, 467–474.

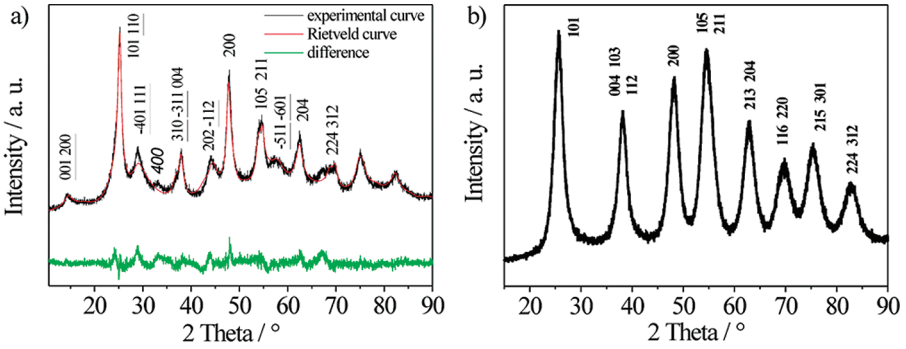

Figure 1. (a) X-ray diffractograms (XRD) and Rietveld analysis of an anatase-TiO_2(B) mixed sample (anatase, 43 wt %; TiO_2(B), 57 wt %) prepared with 10 wt % C_{16}mimCl in C_4mimBF_4 (sample 2 in Table 1). The underlined indices indicate TiO_2(B) (JCPDS number 35−0088) and the plain indices anatase (JCPDS number 21−1272). (b) XRD pattern of a pure anatase sample, which was prepared in a mixture of 40 wt % C_{16}mimCl in EAN (sample 25 in Table 1).

harmonics model. The results of the Rietveld analysis are summarized in Table 1. Interestingly, the anatase crystallites (average values) are significantly bigger than the TiO_2-(B) crystallites, which are only ca. 2 nm in size. Next to it, the size of the anatase crystallites varies between 6 and 9 nm, irrespective of whether anatase is the solely product or together in a mixture with TiO_2(B). Therefore, the presence of a surfactant in the reaction mixture does not influence the particles size of anatase, but more importantly leads to the development of a second phase, e.g., TiO_2(B).

It is interesting to note that the synthesis of titania in EAN in the presence of CTAC or C_{16}mimCl (sample 21−31, Table 1) leads to very small anatase crystallites with an average crystallite size of below 4 nm. Figure 1b shows a XRD pattern of a pure anatase sample synthesized with 40 wt.-% of C_{16}mimCl in EAN. The intensity of the (004) reflection is slightly higher than usual, which accounts for an anisotropic particle morphology. This is further confirmed by Rietveld analysis, which gives a particle size of roughly 4 nm for (004), whereas it is around 3 nm for (101).

The XRD data indicate a high degree of crystallinity of at least ca. 90%. This interpretation is based on the fact that generally a significant portion (i.e., >15 vol %) of amorphous TiO_2 should result in a broad scattering maximum. The absence of such broad maximum allows the conclusion that the crystallinity is at least ca. 90%. This interpretation is supported by the high reversibility observed in cyclic voltammetry (see electrochemical measurements section below).

Low-magnification TEM images support the presence of small homogeneous titania particles for all samples (Figure 2). Figure 2b displays the HRTEM image of a mixed antase-TiO_2(B) sample (composition 53% anatase, 47% TiO_2 (B), sample 5 in Table 1), which proves the high crystallinity of the sample. The analysis of the HRTEM image has been performed by analyzing its corresponding FFT (Figure 2c) of the area inside the black frame in Figure 2b). Accordingly, the spotty FFT pattern indicates mutual alignment of the corresponding analyzed anatase nanoparticle. The symmetry of the spots and the assigned *d*-values points to orientation of the crystallite along the anatase *b*-axis with respect to the electron beam as nicely illustrated in Figure 2c. Also the presence of TiO_2(B) can be traced in Figure 2b, as illustrated by the enhanced lattice planes belonging to the (001) direction of TiO_2(B).

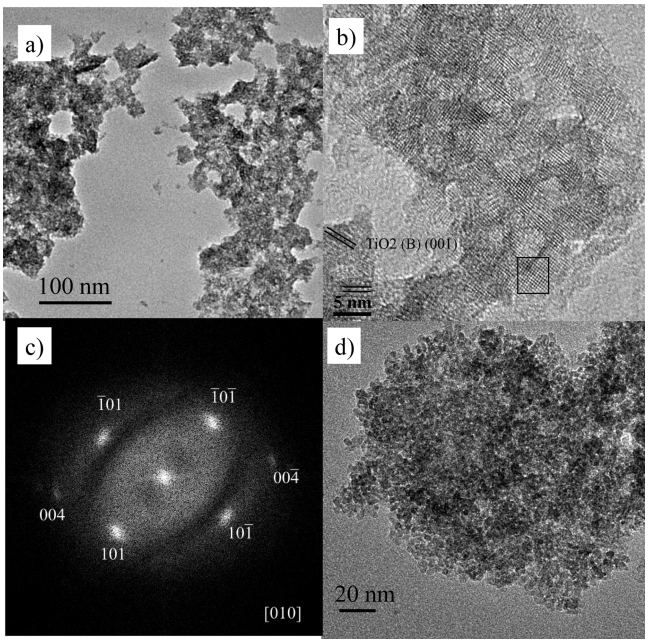

Figure 2. (a) Low- and (b) high-resolution transmission electron microscopy (TEM) of an anatase-TiO_2(B) sample (composition: 53% anatase, 47% TiO_2(B), sample 5 in Table 1). (c) Fourier transfomation of the black rectangular in b. (d) Low-magnification TEM of a pure anatase sample (sample 22 in Table 1).

Figure 2d shows the low-magnification TEM image of a pure anatase sample (sample 22 in Table 1).

Another interesting feature seen in these TEM analyses is the spongelike mesopore structure (see Figure 2b), which is associated with the mutual alignment of the nanocrystals. Because no structure-directing agent is added being capable to template such large pores (e.g., a block copolymer), these "mesopores" do not result from a 1:1 replication process, but are generated during the peculiar crystallization into aligned nanocrystals. Most probably, the mesopores correspond to nanosized domains of ionic liquid/surfactant created during the condensation/crystallization of titanium dioxide clusters into TiO_2(B). After washing, these phase-separated IL domains are converted into a corresponding mesopore.

Because the electrochemical characterization had to be conducted on FTO substrates, in a series of experiments, the influence of the substrates and heat treatment temperature was investigated: Although the advantage of the

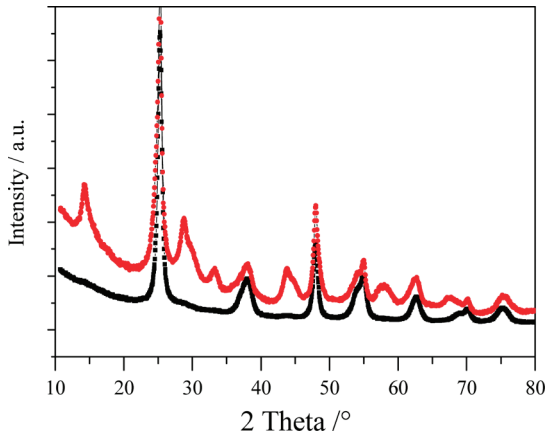

Figure 3. XRD patterns of a material corresponding to sample 5, treated at T = 400 °C for 1 h. Red curve: sample 5 with surfactant (Triton) and acetyl acetonate on FTO substrate. Black curve: sample 5 with surfactant (Triton) and acetyl acetonate in a ceramic container.

synthetic approach presented lies with the low temperature required, the material prepared at T = 80−100 °C appeared to be unsuitable for electrochemical measurements when directly deposited on FTO substrates, for instance, because of insufficient adhesion to the FTO substrates. Instead, a minimum temperature of T = 400 °C was needed for FTO plates covered by the material (see Figure 3).

It is seen that the substrate exerts a distinct influence on the material. The addition of surfactant (Triton) and acetylacetonate (acac) was needed to ensure good adhesion to the FTO substrate, and in this case no transformation of TiO_2(B) into anatase was observed even at T = 400 °C (Figure 3). By contrast, the heating of sample 5 the same surfactants within a standard container made of ceramics resulted in the complete conversion into anatase. Thus, the heat-treated material used for the electrochemical characterization corresponded to the as-prepared material regarding the phase composition of TiO_2.

2.3. Nitrogen Physisorption. In Table 2, nitrogen sorption data as received from nitrogen sorption measurements at 77 K are presented. It should be emphasized that the materials were measured by physisorption in the state after washing and dried under vacuum at 120 °C. The surface area as determined from Brunauer−Emmett−Teller (BET) analysis of the obtained titania is generally quite high, e.g., above 200 m^2/g. Interestingly, the influence of additives such as CTAC or C_{16}mimCl not only influences the crystallization but also leads to a higher surface area.

Samples that consist of mixtures of anatase and TiO_2-(B) follow the classical type IV nitrogen sorption isotherm with a H3-type hysteresis, which is typical of mesoporous materials (Figure 4a).[28] The average mesopore size was determined using the Barrett−Joyner−Halenda (BJH) approach from the desorption branch. The values for the average pore size (ca. 4 − 10 nm) correspond well with TEM analysis. The pure anatase samples synthesized in

(28) Sing, K. S. W.; Everett, D. H.; Houl, R. A. W.; Moscou, L.; Pierotti, R. A.; Rouquerol, J.; Siemieniewska, T. *Pure Appl. Chem.* **1985**, *57*, 603–619.

Table 2. Nitrogen Sorption Data of Titania Samples Synthesized in C_{16}mimCl/C_4mimBF_4, CTAC/C_4mimBF_4, C_{16}mimBF_4/C_4mimBF_4, C_{16}mimCl/EAN, and CTAC/EAN

sample	wt % surfactant	BET surface area (m^2/g)[a]	BJH(des) pore size (nm)[b]	pore volume (cm^3/g)[c]
		C_{16}mimCl + C_4mimBF_4		
1	0	113	13	0.31
2	10	242	4	0.2
3	20	390	9	0.1
4	30	310	6	0.18
5	40	312	11	0.14
6	50	232	9	0.25
7	60	151	10	0.37
8	70	270	7	0.39
		CTAC + C_4mimBF_4		
9	10	170	4	0.13
10	20	325	4	0.2
11	30	252	8	0.37
12	40	168	5	0.3
13	50	172	9	0.19
14	60	141	9	0.3
15	70	169	11	0.3
		C_{16}mimBF_4 + C_4mimBF_4		
16	10	191	9	0.36
17	20	201	5	0.22
18	30	137	4	0.14
19	40	177	4	0.19
20	50	153	5	0.21
		C_{16}mimCl + EAN		
21	0	297	4	0.19
22	10	337	4	0.23
23	20	325	4	0.2
24	30	355	4	0.25
25	40	359	4	0.26
26	50	398	4	0.24
		CTAC + EAN		
27	10	290	4	0.19
28	20	292	4	0.16
29	30	349	5	0.45
30	40	334	4	0.27
31	50	326	4	0.21

[a] The Brunauer−Emmett−Teller (BET) surface area was determined from the first points of the isotherm up to a relative pressure of p/p_0 = 0.3. [b] The Barrett−Joyner−Halenda (BJH) pore size was determined from the maximum of the pore size distribution determined from the desorption branch. [c] The pore volume was determined from the maximum of the isotherm at p/p_0 = 0.98.

EAN (sample 21−31, Table 2) have a different shape regarding the isotherm (Figure 4b). Unexpectedly, these samples also possess a very high surface area of up to 400 m^2/g (sample 26, Table 2). Even though in these cases the surfactant does not influence the synthesis toward the evolution of the TiO_2(B) polymorph, the surface area is affected by the addition of surfactants, which is presumably due to the described effect of textural alignment of the primary units toward aligned crystalline scaffolds. As seen from Table 2, the surface area increases with increasing amount of surfactant in the initial reaction mixture.

2.4. SAXS. SAXS investigations (Figure 5) of C_{16}mimCl in C_4mimBF_4 at T = 90 °C reveal that mainly one phase is dominant over a broad range of concentrations. Apparently, self-assembled structures—whether micellar or rather randomly assembled—appear at a concentration as low as 8 wt % and dominate the phase diagram until ca. 80 wt %.

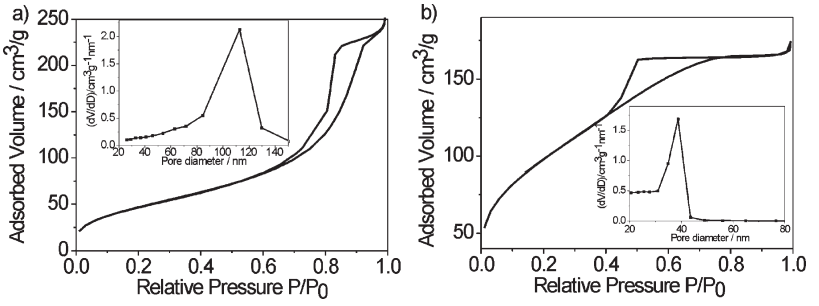

Figure 4. Nitrogen sorption isotherm of (a) sample 5 (anatase/TiO_2(B) = 53/47) and (b) sample 19 (pure anatase, prepared with 40 wt % C_{16}mimCl in EAN) in Table 1. The insets show the Barrett−Joyner−Halenda pore size distribution determined from the desorption branch of the respective sample.

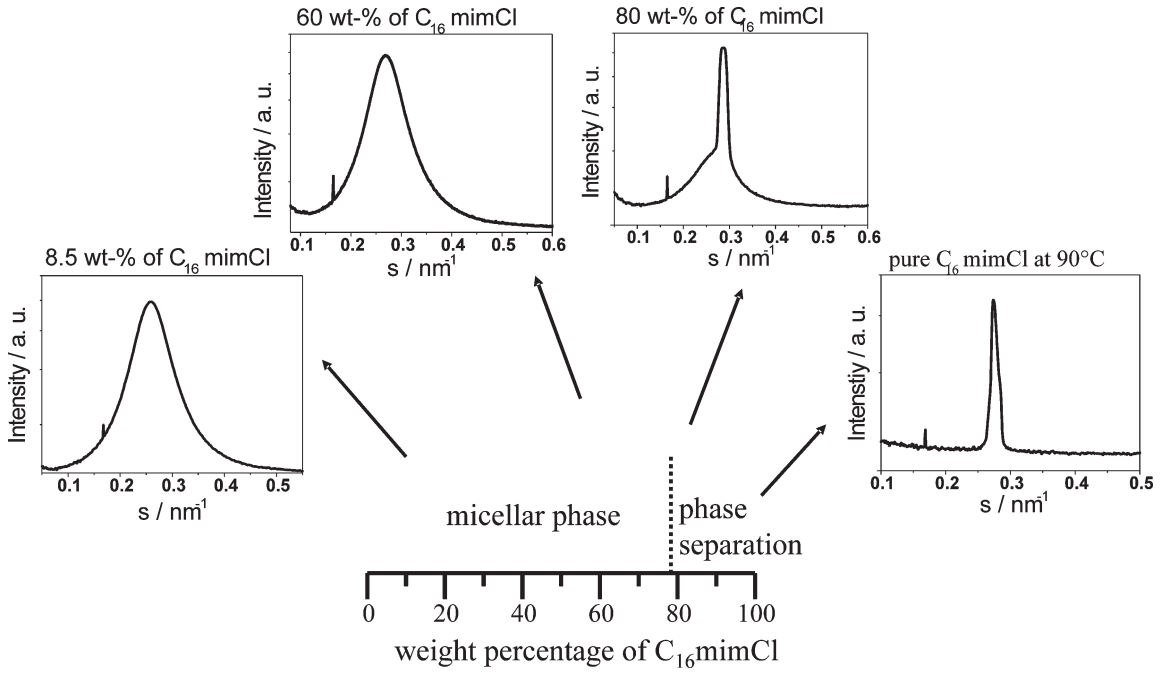

Figure 5. Phase diagram of C_{16}mimCl in C_4mimBF_4 at 90 °C as determined by small-angle X-ray scattering.

Above this concentration, phase-separation is observed, with 100% C_{16}mimCl finally leading to a lamellar thermotropic phase, as described in ref 29. A similar phase behavior is observed for CTAC in C_4mimBF_4 (results not shown). In this case, however, phase separation starts at a lower concentration, e.g., at around 70 wt % of CTAC.

When looking at the reaction mixture under synthesis conditions, e.g., upon the addition of $TiCl_4$ and H_2O, the SAXS pattern does not show any significant changes. As a conclusion, the mixture of C_{16}mimCl in C_4mimBF_4 leads to the formation of self-assembled structures, most likely micelles with a liquid-like packing. The appearance of the TiO_2(B) phase during the synthesis of TiO_2 in such a system does only correlate to a certain extent with the observation of these self-assembled structures. At higher concentration of surfactant, the system becomes very viscous, which also influences the synthesis of titania.

2.5. Electrochemical Characterization. In our study, Li-insertion experiments are used as characterization method to further confirm the presence of two polymorphs of TiO_2. Next to that, the potential of TiO_2 as electrode material for the Li-ion battery can be further explored. In Figure 6, the cyclic voltammograms (CV) of an anatase-TiO_2(B) mixture with a composition of ca. 53% anatase and 47% TiO_2(B) (determined by XRD analysis), (sample 5 in Table 1) is shown, measured at a scan rate of 10 mV s^{-1}.

The first cycle shows electrochemical response of both modifications, anatase (anodic peak at 2.38 V) and TiO_2-(B) (anodic peak at 1.84 V). These values are similar to those observed in the literature for anatase and TiO_2(B) under equivalent experimental conditions.[30] We attribute the broadness of the anatase anodic peak and the $\Delta E_{\text{anatase}} = 1.17$ V ($\Delta E = E_{\text{cathodic peak}} - E_{\text{canodic peak}}$) to the deposition process of titania powder on the FTO substrate. This method allows only for a reduced contact between the particles and consequently the electronic propagation through the material is aggravated. The broad cathodic peak is characteristic of a hybrid anatase-TiO_2(B) material. The evolution of the CV profile upon repeated cycling shows a significant decrease of the anatase and TiO_2(B) anodic peaks. Apparently, TiO_2(B)

(29) Kaper, H.; Smarsly, B. *Z. Phys. Chem.* **2006**, *220*, 1455–1471.

(30) Fattakhova-Rohlfing, D.; Wark, M.; Brezesinski, T.; Smarsly, B. M.; Rathousky, J. *Adv. Funct. Mater.* **2007**, *17*, 123–132.

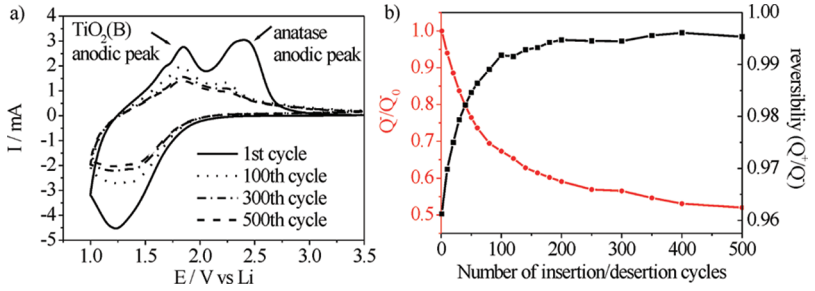

Figure 6. (a) Cyclic voltammetry of a sample containing 53% anatase and 47% TiO_2(B) (sample 5 in Table 1). Scan rate: 10 mV s^{-1}. Solid line, 1st cycle; dotted line, 100th cycle; dash-dot, 300th cycle; dashed, 500th cycle. (b) Extracted values from panel a. Evolution of inserted charge Q^- upon cycling vs first cycle Q^-_0 (red line) and reversibility, e.g., charge extracted Q^+/charge-inserted Q^-, (black curve).

nanoparticles exhibit a better stability than the anatase nanoparticles, an observation that agrees well with literature.[13,16]

From the integrated area under the anodic peaks, the relative amount of anatase to TiO_2(B) can be determined. In our case, the integration of the TiO_2(B) and anatase anodic peaks gives a ratio of 40/60. This value slightly differs from the 50/50 ratio obtained from XRD data. We attribute this difference to a size factor, as TiO_2(B) particles are much smaller (ca. 2 nm) than anatase nanoparticles, and at such small nanoscale size can generates an extra effect on the electrochemical performances.[31]

Upon repeated cycling the total amount of charge exchange decreases (Figure 6), which is usually observed in electroactive materials,[16] as the number of active sites for reversible Li^+ trapping is slowly decreasing. After 450 cycles, the total amount of charge inserted during the reduction step (Q^-) reaches a plateau at roughly 50% of the initial value Q^-_0. The anatase anodic peak intensity value passes from 2.75 mA (1st cycle) to 1 mA (500th cycle), corresponding to a loss of 64%. In comparison, the TiO_2(B) anodic peak decreases from 2.05 mA to 1.4 mA, the loss is limited to 31%. The high reversibility of up to 95% proves the absolute dry experimental conditions so that cross reaction with water or oxygen can be excluded. Next to that, the high reversibility accounts for a high crystallinity of the material.

The galvanostatic measurement (Figure 7a) is similar to the superposition of the galvanostatic response for pure anatase[32,33] and pure TiO_2(B), measured with a scan rate of $C/1$ between 1.15 and 2.5 V versus Li.[3] The minimum potential value is limited to $E = 1.15$ V and the material reaches a Li^+ doping value of $x = 0.64$ (215 mA h g^{-1}). This charge capacity is the combination of the total charge capacity from anatase and TiO_2(B) as confirmed by the derivation of the galvanostatic measurement (Figure 6 b). The curve presents two pairs of redox peaks between 1.5 to 2 V:

The first pair (anodic peak 1.95 V, cathodic peak 1.74 V) is typical of anatase and corresponds to a transition from tetragonal $Li_{0.05}TiO_2$ to orthorhombic $Li_{0.5}TiO_2$ during Li^+ insertion.[32] For this potential, Li^+ insertion occurs also in TiO_2(B), but no characteristic structural change was described in the literature.[12]

The second pair (anodic peak 1.6 V, cathodic peak 1.68 V) is the main one observed for TiO_2(B), and for this process no characteristic structural change occurs during Li^+ insertion/extraction. At this potential, anatase is considered to be saturated and reversible insertion/extraction occurs only in TiO_2(B) nanoparticles.

The total discharge capacity is only $x = 0.49$ (165 mA h g^{-1}), but such low reversibility can be related to the imperfect assembly of material in the electrochemical cell.

In general, the degree of lithiation/delithiation can be a function of the scan rate, because Li^+ diffusion into anatase is slower than into TiO_2(B). Accordingly, it is possible that the phase ratio determined by XRD differs from that determined based on electrochemical measurements. The material of sample 5 was thus also studied at a scan rate of 0.1 mV/s. It is seen (see Figure 8) that the integration of the peaks origination from the anatase and TiO_2(B) phase result in a ratio of 56/44, respectively, in good agreement with the Rietveld analysis of XRD data.

3. Conclusion

In this study, we investigated the crystallization behavior of titania in binary mixtures of an ionic liquid with a surfactant or another ionic liquid, especially a long-chain surfactant in a short-chain ionic liquid. Ionic liquids by themselves offer already a unique crystallization environment, which in certain cases allows the facile synthesis of novel or difficult to synthesize materials.[17] By dissolving a surfactant in the ionic liquid, the crystallization behavior of titania is altered, which most likely is due to the presence of self-assembled aggregates promoting nucleation. We observed the formation of the peculiar TiO_2(B) phase next to anatase, and the content of TiO_2(B) in the final product can reach values up to 60%. So far, we can only speculate about the mechanism resulting in the crystallization of this desired titania phase, but our systematic series of experiments presented at least indirect insights into the generation of TiO_2(B). As the size of anatase crystals practically does not change with surfactant concentration, we can exclude surface modification or even inhibition of the anatase phase. Here, the small nanoparticles seem to be similarly stabilized both by the

(31) (a) Wang, J.; Polleux, J.; Lim, J.; Dunn, B. *J. Phys. Chem. C* **2007**, *111*, 14925–14931. (b) Brezesinski, T.; Wang, J.; Polleux, J.; Dunn, B.; Tolbert, S. H. *J. Am. Chem. Soc.* **2009**, *131*, 1802–1809.
(32) Yamada, H.; Yamato, T.; Moriguchi, I.; Kudo, T. *Solid State Ionics* **2004**, *175*, 195–198.
(33) Moriguchi, I.; Hidaka, R.; Yamada, H.; Kudo, T. *Solid State Ionics* **2005**, *176*, 2361–2366.

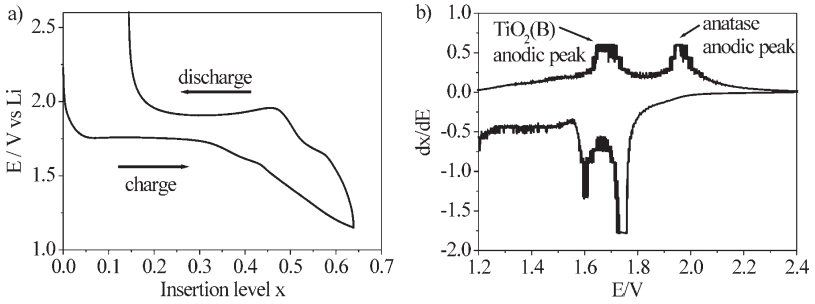

Figure 7. (a) Galvanostatic insertion and desertion curve of a sample containing 53% anatase and 47% TiO_2(B) (sample 5 in Table1) measured at a scan rate of *C*/1 (charge/discharge of cell capacity in 1 h) between 1.15 and 2.5 V (versus Li). (b) Derivative obtained from Figure 6a.

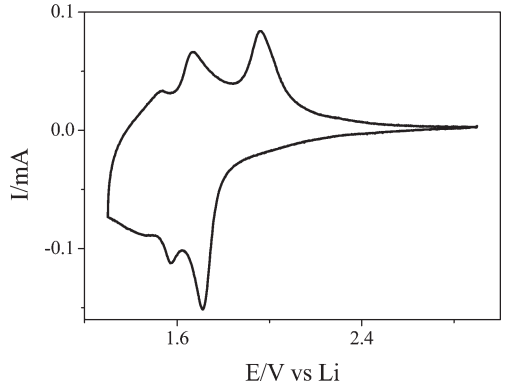

Figure 8. Cyclic voltammetry of a sample corresponding to sample 5 in Table 1 with a scan rate of 0.1 mV s^{-1}. Integration of the anatase and TiO_2(B) anodic peaks gives a ratio of 56/44, respectively, which is quite close to the values obtained from XRD.

solvent and the surfactant. On the contrary, TiO_2(B) seems to have a enhanced nucleation rate, presumably from interface between the surfactant micelles and the IL "solvent", which in addition has to be constituted from imidazolium moieties. Thus, it seems to be a peculiar charge distribution and polarization pattern created by surfactant self-assembly that seems to favor the formation of TiO_2(B). The details of this interaction, however, have to be addressed in further studies using direct and in situ methods.

For the anatase samples, we can additionally observe an interesting pore formation mechanism, in which the single nanoparticles vectorially align toward crystalline scaffolds with clearly nonstatistical crystal orientation and interstitial pore sizes, which has not been observed in "single-IL-syntheses".[20] It is an open question on how much the surfactant assemblies support this scaffolding by a tectonic support mechanism; in any case, they provide a sufficient mobility to the nanoparticles to allow the energetic optimization of mutual orientation. This phenomenon was recently described as a general scheme in the crystallization of diverse oxides in the presence of certain charged organic additives.[34]

The electrochemical experiments confirm the presence of the two titanium dioxide species, namely anatase and TiO_2(B). The electrochemical response intensity of each phase is influenced by the ratio of the phases and the size of the nanocrystallites. The nanosized TiO_2(B) appears to be superior and therefore an attractive material for Li-insertion, because the charge capacity is higher and the electrochemical stability is improved in direct side-by-side comparison to nanocrystalline anatase.

Although it is certainly desirable to synthesize phase-pure TiO_2(B) nanoparticles from a fundamental point of view, recent publications have demonstrated that for electrochemical applications anatase/TiO_2(B) mixtures may even advantageous compared to pure TiO_2(B). Li et al. showed that anatase/TiO_2(B) core−shell nanofibers possess quite promising photocatalytic activity because of an enhanced charge mobility at the interface between anatase and TiO_2(B).[35]

Moreover, our results and recent findings of Procházka et al. on mesoporous templated TiO_2(B) indicate that, in contrast to the hydrothermal methods described in the Introduction, sol−gel processes starting from molecular TiO_2 precursors ($TiCl_4$, etc.) always provide mixtures of TiO_2(B) and anatase.[36]

Thus, further studies will be dedicated to achieving a higher content of TiO_2(B) and the study of electrochemical properties in terms of lithium insertion.

4. Experimental Section

Synthesis of TiO_2(B)/Anatase Mixtures. In a typical synthesis, first the solvent mixture of surfactant and IL was prepared. Thus, the weighed amount of CTAC or C_{16}mimCl was added to the weighed amount of the respective IL (e.g., C_4mimBF_4 and EAN), so that the total amount of surfactant/IL mixture yielded 1 g. The mixture was heated to 100 °C under magnetic stirring until a clear, homogeneous solution was obtained. In a second step, 0.2 mL of $TiCl_4$ (1.8 mmol) was slowly added. ***Caution!*** *$TiCl_4$ is highly corrosive and reacts violently with water*. The solution turned yellow. After 2 min, 0.2 mL of distilled H_2O was added dropwise. The reaction mixture was stirred for 14 h overnight. To remove the Il and the solvent, the reaction mixture was extracted in excess ethanol at 80 °C for 8 h. Finally, the product was collected by centrifugation and repeated washing with ethanol for three times. The obtained white powder was dried at 80 °C prior to further analysis.

Preparation of the Electrodes. First, the TiO_2 powder was grained in a ball mill for 20 min. Then, 0.1 g of TiO_2 powder was

(34) Antonietti, M.; Niederberger, M.; Smarsly, B. M. *Dalton Trans.* **2008**, *1*, 18–24.

(35) Li, W; Liu, C.; Zhou, Y.; Bai, Y.; Feng, X.; Yang, Z.; Lu, L.; Lu, X.; Chan, K.-Y. *J. Phys. Chem. C* **2008**, *112*, 20539–20545.

(36) Prochazka, J.; Kavan, L.; Zukalova, M.; Frank, O.; Kalbac, M.; Zukal, A.; Klementova, M.; Carbone, D.; Graetzel, M. *Chem. Mater.* **2009**, *21*, 1457–1464.

mixed with 0.05 mL of Triton X and 0.05 mL of acetylacetonate. The solution was diluted with ethanol and mortared until a homogeneous paste was obtained. The dispersion was spin-coated on FTO wafers and sintered at 400 °C for 30 min on air.

Before use, the samples were dried in a vacuum oven (pressure below 1 mbar) at 130 °C overnight. Electrochemical measurements were performed in an Ar-filled glovebox (O_2 and H_2O below 1 ppm) using Autolab 302 potentiostat/glavanostat (Eco Chemie). As electrolyte solution served a 1.0 M $LiN(-SO_2CF_3)_2$ (provided from Aldrich) solution in 1:1 w/w mixture of anhydrous EC:DME (ethylene carbonate, Aldrich, 1,2 dimethoxyethane Fluka). Titanium dioxide on FTO glasses were used as working electrode, platinum wire as counter electrode, and Li foil as reference electrode. After measurement, the samples are washed with ethanol, sintered at 550 °C for 4 h, and then scratched off with a razor blade and weight lost was measured.

Characterization. Transmission electron microscopy (TEM) as well as high-resolution transmission electron microscopy (HRTEM) characterization was performed on a CM30ST microscope (Philips; LaB_6 cathode, operated at 300 kV, point resolution of 2 Å). For TEM and HRTEM characterization, the dried sample was thoroughtly sonicated. One drop of this suspension was placed on a 400-mesh carbon-coated copper grid and left in air to dry.

Nitrogen sorption experiments were performed on a Micromeritics Tristar 3000 automated gas adsorption analyzer. Prior to sorption measurements, the samples were degassed in a Micromeritics VacPrep061 degasser overnight at 100 °C under 100 μTorr pressure.

X-ray Diffraction merasurements were conducted on a D8 diffractometer from Bruker instrument (wavelength 0.154 nm) as well as on a Siemens D5005 diffractomenter.

Acknowledgment. H.K. thanks the Institute of Bioengineering and Nanotechnology (Biomedical Research Council, Agency for Science, Technology and Research, Singapore) for support and funding.